## Topological theory of resilience and failure spreading in flow networks

Franz Kaiser \* and Dirk Witthaut

Forschungszentrum Jülich, Institute for Energy and Climate Research (IEK-STE), 52428 Jülich, Germany and Institute for Theoretical Physics, University of Cologne, 50937 Köln, Germany

(Received 11 September 2020; accepted 7 May 2021; published 1 June 2021)

Link failures in supply networks can have catastrophic consequences that can lead to a complete collapse of the network. Strategies to prevent failure spreading are thus heavily sought after. Here, we make use of a spanning tree formulation of link failures in linear flow networks to analyze topological structures that prevent failure spreading. In particular, we exploit a result obtained for resistor networks based on the *matrix tree theorem* to analyze failure spreading after link failures in power grids. Using a spanning tree formulation of link failures, we analyze three strategies based on the network topology that allow us to reduce the impact of single link failures. All our strategies either do not reduce the grid's ability to transport flow or do in fact improve it—in contrast to traditional containment strategies based on lowering network connectivity. Our results also explain why certain connectivity features completely suppress any failure spreading as reported in recent publications.

DOI: 10.1103/PhysRevResearch.3.023161

#### I. INTRODUCTION

The theory of linear flow networks provides a powerful framework, allowing one to study systems ranging from water supply networks [1,2] and biological networks, such as leaf venation networks [3–6], to resistor networks [7–9], or ac power grids [10,11]. Failures of transportation links in these networks can have catastrophic consequences up to a complete collapse of the network. As a result, link failures in linear flow networks and strategies to limit their consequences are a field of active study [12–19].

The study of linear flow networks is intimately related to graph theory since most phenomena can be analyzed on purely topological grounds [7]. This connection dates back to work by Kirchhoff [8], who analyzed resistor networks and introduced several major tools that are now the basis of the theory of complex networks, such as the matrix tree theorem [7,8,20]. These tools can now serve as a basis for the analysis of failure spreading in ac power grids, which can be modeled as linear flow networks based on the dc approximation [11]. A substantial part of security analysis in power grids is dedicated to the study of transmission line outages since they can lead to cascading outages in a series of failures [21–23].

The topological approach to failure spreading has been exploited to demonstrate that the strength of flow rerouting after link failures decays with distance to the failing link [12–15]. In particular, the so-called rerouting distance based

Published by the American Physical Society under the terms of the Creative Commons Attribution 4.0 International license. Further distribution of this work must maintain attribution to the author(s) and the published article's title, journal citation, and DOI.

on cycles in the network has been found to predict flow rerouting very well [12]. However, the analysis of flow rerouting still lacks a theoretical foundation. Here, we demonstrate that these observations made for flow rerouting may be understood based on a formalism originally developed to study current flows in resistor networks that uses spanning trees (STs) of the underlying graph. Moreover, the formalism explains recent results regarding the shielding against failure spreading in complex networks.

This paper is structured as follows. In Sec. II, we give an overview over the theory of linear flow networks and present an important lemma that relates the current flows in these networks to STs. In Sec. III, we demonstrate the analogy between such networks and ac power grids in the dc approximation and relate the ST formulation to line outages studied in power system security analysis. Finally, in Sec. IV we show how this formulation may be used to understand why certain connectivity features inhibit failure spreading extending on recent results [19].

#### II. FUNDAMENTALS OF RESISTOR NETWORKS

Resistor networks are a prime example of linear flow networks and have inspired research throughout centuries [7,8,24]. A resistor network can be described using a graph as follows. Let G = (E, V) be a connected graph with vertex set  $V = \{v_1, \ldots, v_N\}$  and M edges in the edge set E. Then we assign a weight  $w_k$  to each edge  $e_k = (a, b)$  in the graph given by the inverse resistance  $w_k = R_k^{-1}$  between its terminal vertices a and b. If there is a potential difference  $v_k = V_a - V_b$  between the terminal vertices of edge  $e_k = (a, b)$ , according to Ohm's law there is a current flow  $i_k$  between the two vertices given by

$$i_k = \frac{v_k}{R_k} = \frac{V_a - V_b}{R_k}. (1)$$

<sup>\*</sup>f.kaiser@fz-juelich.de

<sup>†</sup>d.witthaut@fz-juelich.de

In order to give a direction to the current flow, we assign an arbitrary orientation to each edge in the graph that is encoded by the graph's edge-node-incidence matrix  $\mathbf{B} \in \mathbb{R}^{N \times M}$  defined as [7]

$$B_{n,\ell} = \begin{cases} 1 & \text{if line } \ell \text{ starts at node } n \\ -1 & \text{if line } \ell \text{ ends at node } n \\ 0 & \text{otherwise.} \end{cases}$$
 (2)

The current flows and voltages are then subject to *Kirchhoff's circuit laws* [8]. The first of the laws, typically referred to as Kirchhoff's current law, at an arbitrary node  $j \in V(G)$  reads as

$$\sum_{e_k \in \Lambda(j)}^M i_k = I_j.$$

Here,  $I_j \in \mathbb{R}$  is the current injected into or withdrawn from node j, and  $\Lambda(j) \subset E(G)$  is the set of all edges that connect to node j respecting their orientation. The current law may be regarded as a continuity equation and thus states that the inflows and outflows at each node in the network have to balance with the current injections at the respective node. It may be written more compactly making use of the node-edge-incidence matrix

$$\mathbf{Bi} = \mathbf{I},\tag{3}$$

where  $\mathbf{i} = (i_1, \dots, i_M)^{\top} \in \mathbb{R}^M$  is a vector of current flows and  $\mathbf{I} = (I_1, \dots, I_N)^{\top} \in \mathbb{R}^N$  is a vector of current injections. On the other hand, we can also introduce a more compact notation for Ohm's law (1) by defining a vector of nodal voltage levels  $\mathbf{V} = (V_1, \dots, V_N)^{\top} \in \mathbb{R}^N$  and a diagonal matrix of edge resistances  $\mathbf{R} = \operatorname{diag}(R_1, \dots, R_M) \in \mathbb{R}^{M \times M}$  such that Ohm's law reads as

$$\mathbf{Ri} = \mathbf{B}^{\top} \mathbf{V}. \tag{4}$$

Combining Ohm's law with Kirchhoff's current law, we arrive at the following relationship between nodal voltages V and nodal current injections I:

$$\mathbf{I} = \mathbf{B} \mathbf{R}^{-1} \mathbf{B}^{\mathsf{T}} \mathbf{V}. \tag{5}$$

This Poisson-like equation has been analyzed in different contexts [7,12,25]. Note that Kirchhoff's voltage law is automatically satisfied by virtue of Eq. (3), because the resulting vector of potential differences  $\mathbf{v} = \mathbf{B}^T \mathbf{V}$  vanishes along any closed cycle due to the duality between the graph's cycle space and its cut space [7,26]. In addition to that, the potential at one node may be chosen freely without affecting the result.

The matrix connecting the two quantities is referred to as a weighted graph Laplacian or Kirchhoff matrix  $\mathbf{L} = \mathbf{B}\mathbf{R}^{-1}\mathbf{B}^{\top} \in \mathbb{R}^{N \times N}$  and characterizes the underlying graph completely. It has the following entries [7]:

$$L_{mn} = \begin{cases} \sum_{\ell \in \Lambda(m)} w_{\ell} & \text{if } m = n \\ -w_{\ell} & \text{if } m \text{ is connected to } n \text{ by } \ell. \end{cases}$$
 (6)

Here, the weight of an edge  $\ell$  is again given by its inverse resistance  $w_{\ell} = R_{\ell}^{-1}$ . For a connected graph, this matrix has exactly one vanishing eigenvalue  $\lambda_1 = 0$  with corresponding unit eigenvector  $\mathbf{v}_1 = \mathbf{1}/\sqrt{N}$  such that  $\mathbf{L}\mathbf{1} = 0$ . For this reason, the matrix is noninvertible. This is typically overcome by

making use of the graph's Moore-Penrose-pseudoinverse  $L^{\dagger}$ , which has properties similar to the actual inverse [27].

With this formalism at hand, we can in principle now determine the current on any edge given a particular injection pattern **I** and edge resistances **R**. As a start, consider the situation where each edge has a unit resistance **R** = diag(1) and a unit current is injected into a particular vertex s and withdrawn at another one t such that  $\mathbf{I} = \mathbf{e}_s - \mathbf{e}_t$ , where  $\mathbf{e}_i = (0, \dots, \underbrace{1}_i, \dots, 0)^{\top} \in \{0, 1\}^M$  are the unit vectors with en-

try one at position i and zero otherwise. In this situation, the current across any edge in the graph  $\ell = (a, b)$  is given by the following lemma, which dates back to Kirchhoff [8,20] and has been popularized by Shapiro [7,28].

Lemma 1. Put a 1-A current between the vertices s and t of a connected, unweighted graph G such that  $\mathbf{I} = \mathbf{e}_s - \mathbf{e}_t$ . Then the current on any other edge (a, b) is given by

$$i_{ab} = \frac{\mathcal{N}(s, a \to b, t) - \mathcal{N}(s, b \to a, t)}{\mathcal{N}},$$

where  $\mathcal{N}(s, a \to b, t)$  is the number of STs that contain a path from s to t of the form  $s, \ldots, a, b, \ldots, t$  and  $\mathcal{N}$  is the total number of STs of the graph.

Whereas this lemma only holds for graphs where all links have unit resistances, real-world resistor networks or other types of linear flow networks are typically weighted with non-homogeneous resistances. However, the extension to weighted networks is straightforward as summarized in the following corollary (see, e.g., Theorem II.2 in Ref. [7]).

Corollary 1. Put a 1-A current between the vertices s and t of a connected, weighted graph G such that  $\mathbf{I} = \mathbf{e}_s - \mathbf{e}_t$ . Then the current on any other edge (a, b) is given by

$$i_{ab} = \frac{\mathcal{N}^*(s, a \to b, t) - \mathcal{N}^*(s, b \to a, t)}{\mathcal{N}^*}, \tag{7}$$

where  $\mathcal{N}^* = \sum_{T \in \mathcal{T}} \prod_{e \in T} w_e$  is the sum over the products of the weights  $w_e$  of all edges  $e \in T$  that are part of the respective spanning tree T;  $\mathcal{T}$  is the set of all STs in the graph. Similarly,  $\mathcal{N}^*(s, a \to b, t)$  equals the sum over all STs that contain a path of the form  $s, \ldots, a, b, \ldots, t$ , where each ST is weighted with the product of the weight  $w_e$  of all edges that are part of it. We thus assign a weight to each ST given by the product of the weights of the edges on the ST and replace the unweighted STs in Lemma 1 by weighted STs.

We will demonstrate in the following sections how this lemma and corollary may be made use of to understand how failure spreading may be mitigated in linear flow networks such as ac power grids in the dc approximation.

# III. ANALOGY BETWEEN RESISTOR NETWORKS AND POWER FLOW IN ELECTRICAL GRIDS

Importantly, the theoretical framework developed in the last section may be applied not only to resistor networks but also to power grids. In this section, we demonstrate how these results may be used to gain insight into the mitigation of failure spreading in power grids.

TABLE I. Analogy between resistor networks and ac power grids in the dc approximation.

dc approximation		Resistor network	
Quantity	Symbol	Quantity	Symbol
Power injections	P	Nodal current	I
Real power flow	$\mathbf{F}$	Current flow	i
Nodal phase angles	$\vartheta$	Nodal voltages	$\mathbf{V}$
Line susceptances	$b_e$	Inverse edge resistance	$r_e^{-1}$

## A. Modeling power grids as linear flow networks

Most electric power transmission grids are made up of ac transmission lines and are, as such, governed by the nonlinear ac power flow equations [11]. However, the real power flow over transmission lines can be simplified to a linear flow model in what is referred to as the dc approximation of the ac power flow. This approximation is based on the following assumptions [29].

- (i) Nodal voltage magnitudes vary little.
- (ii) Transmission lines are purely inductive; that is, their resistance is negligible compared with their reactance  $r_{\ell} \ll x_{\ell}$ ,  $\forall \ell \in E(G)$ .
- (iii) Differences between nodal voltage angles  $\vartheta_n$ ,  $n \in V(G)$ , of neighboring nodes n, m are small  $|\vartheta_n \vartheta_m| \ll 1$ .

Typically, these assumptions are met if the power grid is not heavily loaded and if the power grid is modeled at the transmission level where line resistances are small [29]. As a result, the real power flow  $F_{\ell}$  along a transmission line  $e_{\ell} = (n, m) \in E(G)$  in the dc approximation depends linearly on the nodal voltage phase angles  $\vartheta_n$  of neighboring nodes

$$F_{\ell} = b_{\ell}(\vartheta_n - \vartheta_m). \tag{8}$$

Here,  $b_\ell \approx x_\ell^{-1}$  is the line susceptance of line  $\ell$ . Thus the vector of real power flow along the transmission lines in the power grid  $\mathbf{F} = (F_1, \dots, F_M)^\top \in \mathbb{R}^M$  takes the role of current flow vector in the case of resistor networks. On the other hand, the nodal voltage phase angles  $\boldsymbol{\vartheta} = (\vartheta_1, \dots, \vartheta_N)^\top \in \mathbb{R}^N$  take the role of the nodal voltages  $\mathbf{V}$ , and line weights are given by the line susceptances  $b_k$  of an edge  $e_k$  in correspondence with the inverse resistances  $R_k^{-1}$  in the case of resistor networks. Thus Ohm's law (4) translates to power grids as

$$\mathbf{F} = \mathbf{B}_d \mathbf{B}^\top \boldsymbol{\vartheta}.$$

Here,  $\mathbf{B}_d = \operatorname{diag}(b_1, \dots, b_M) \in \mathbb{R}^{M \times M}$  is the diagonal matrix of line susceptances. Again, Kirchhoff's current law (3) holds, and we may express it using vector quantities as follows [11,12]:

$$BF = P$$
.

Here,  $\mathbf{P} = (P_1, \dots, P_N)^{\top} \in \mathbb{R}^N$  is the vector of nodal power injections, which thus takes the role of nodal current injections **I**. We summarize these equivalences in Table **I**.

### B. Sensitivity factors in power grid security analysis

In power grid security analysis, linear sensitivity factors are used to study and prevent line overloads which could cause disturbances to power system operation and result in power outages [11]. One of these factors is the *power transfer* distribution factor (PTDF). The PTDF<sub>s,t,k</sub> then quantifies the change in flow  $\Delta F_k$  on line  $e_k \in E(G)$  if a power  $\Delta P$  is injected at node r and withdrawn from node s. It is calculated as [11]

$$PTDF_{r,s,k} = \frac{\Delta F_k}{\Delta P}.$$
 (9)

Now assume that a single line  $e_m$  fails, for example, as a result of an overload, and is disconnected from the network. The change in power flow on a line  $e_k$  may then be calculated by using the *line outage distribution factor* (LODF) [11]

$$LODF_{k,m} = \frac{\Delta F_k}{F_m^{(0)}}.$$
(10)

Here,  $F_m^{(0)}$  is the flow on line  $e_m$  before the outage. Mathematically, we can map the flow changes after a failure to the flow changes after changes in the injection patterns by considering power injections that effectively compensate for the flow on the link that is assumed to fail (see Refs. [11,12]). As a result, the two quantities are related as follows if  $e_m = (r, s)$  is the failing link [11]:

$$LODF_{k,m} = \frac{PTDF_{r,s,k}}{1 - PTDF_{r,s,m}}.$$
 (11)

Note that the description of link failures using LODFs relies on the dc approximation of the nonlinear ac power flow equations. However, extended descriptions have been proposed that incorporate nonlinear terms [31]. Furthermore, the dc approximation and thus the LODF-based description of link failures are commonly used to model cascading failures in power grids, where a single link triggers the failure of other links [23,32,33]. A comparison of the effect of link failures in linear and nonlinear models of power flows can, for example, be found in Ref. [34].

## C. Spanning tree description of link failures

On the basis of the analogy between electrical grids and resistor networks developed in the last sections, we will now show how the ST formula presented in Corollary 1 may be used for power system security analysis. In the language of power grids, the lemma yields the PTDF<sub>s,t,m</sub> for an edge  $e_m = (a, b)$  if a unit power  $\Delta P$  is injected at node r and withdrawn from node s. For this reason, the PTDF may be calculated as follows:

$$PTDF_{s,t,m} = \frac{\mathcal{N}^*(s, a \to b, t) - \mathcal{N}^*(s, b \to a, t)}{\mathcal{N}^*}.$$
 (12)

Based on Eq. (11), which yields the LODF expressed in terms of the PTDF, we can make use of this expression to derive an equivalent expression for the LODF. If  $e_k = (r, s)$  is the failing link and  $e_m = (a, b)$  is the link where the flow changes are monitored, the expression based on Eq. (12) reads as

$$LODF_{m,k} = \frac{\mathcal{N}^*(r, a \to b, s) - \mathcal{N}^*(r, b \to a, s)}{\mathcal{N}^* - [\mathcal{N}^*(r, r \to s, s) - \mathcal{N}^*(r, s \to r, s)]}$$

$$= \frac{\mathcal{N}^*(r, a \to b, s) - \mathcal{N}^*(r, b \to a, s)}{\mathcal{N}^* - \mathcal{N}^*(r, r \to s, s)}$$

$$= \frac{\mathcal{N}^*(r, a \to b, s) - \mathcal{N}^*(r, b \to a, s)}{\mathcal{N}^*_{\{k\}}}.$$
 (13)

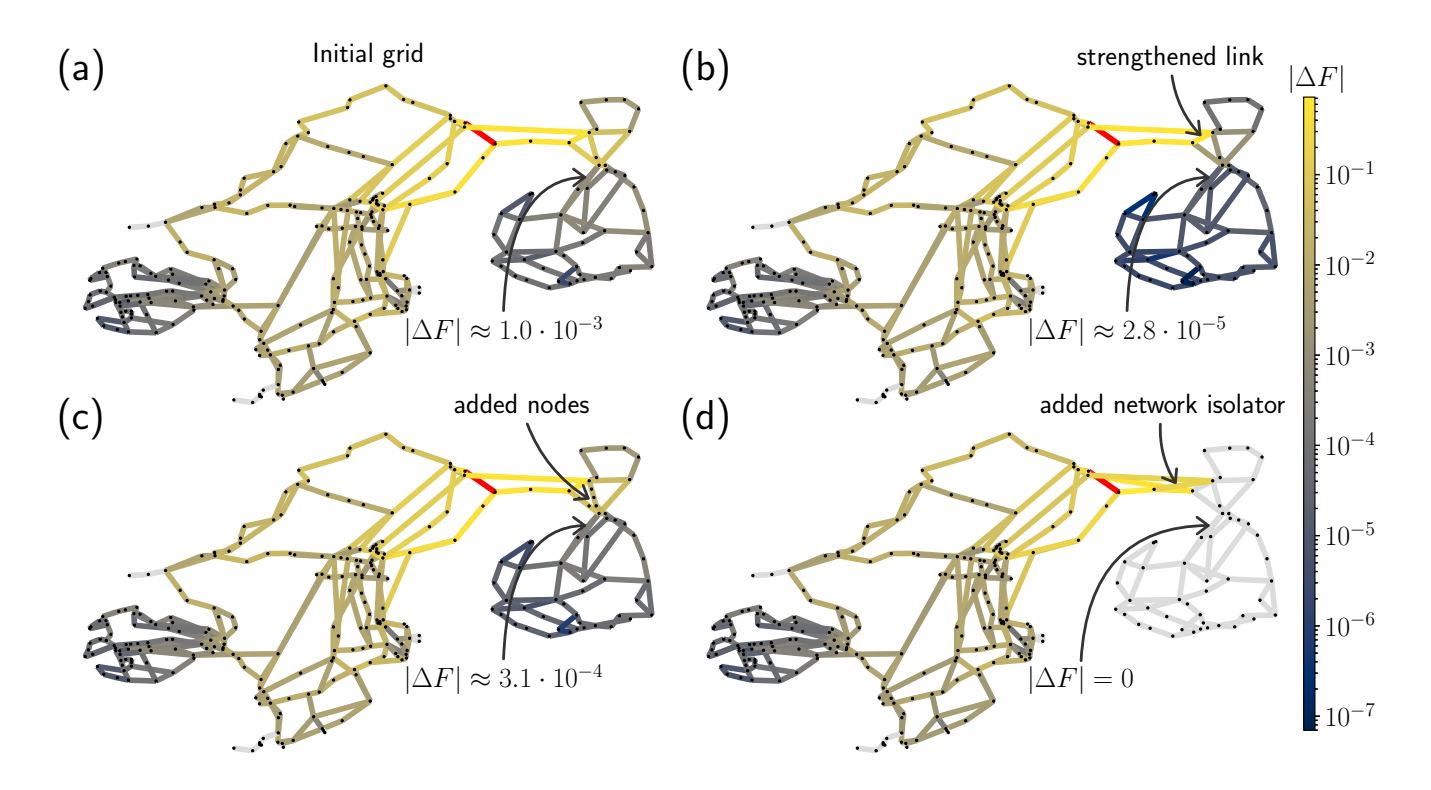


FIG. 1. Different methods for mitigating failure spreading in linear flow networks. (a) The failure of a single link (red) with unit flow results in flow changes  $\Delta F$  (color scale) throughout the Scandinavian power grid. (b) Failure spreading to Finland may be reduced by strengthening a link that horizontally separates Sweden and Finland. (c) Adding nodes, thus increasing the length of the rerouting path, reduces failure spreading to Finland as well. (d) Adding two links to construct a network isolator results in a complete vanishing of flow changes in the other part of the grid. Grid topology was extracted from the open energy system model PyPSA-Eur [30].

Here,  $\mathcal{N}^*_{\backslash \{k\}}$  denotes the weight of all STs in the graph evaluated *after* removing the edge  $e_k$  from the set of trees  $\mathcal{T}$ . We thus found an expression for the LODFs that is based purely on certain STs in the graph. This equation is the basis of our analysis of subgraphs inhibiting failure spreading which we will perform in the following sections. Note that a similar expression for the LODFs based on spanning 2-forests has recently been derived by Guo *et al.* [16].

### IV. MITIGATING FAILURE SPREADING

We have seen in the last section that the spreading of failures is studied using LODFs in power system security analysis. To prevent large flow changes on other links after the failure of a link  $e_k$  which may potentially trigger dangerous cascades of failures, it is desirable for overall power system security to keep the LODFs small. A natural question to ask is thus the following: Can we design or alter the network topology in such a way that LODFs stay small? Based on Eq. (13) expressing the LODF in terms of STs, this question may be addressed in a purely topological manner. In particular, we deduce three strategies to reduce the effect of failure spreading.

- (1) Fixing long paths between trigger link  $e_k$  and monitoring link  $e_l$  leaves only few degrees of freedom, which reduces the relative contribution of the numerator in Eq. (13).
- (2) Fixing specific paths between trigger link  $e_k$  and monitoring link  $e_l$  can force links of large weights to be not

contained in the numerator, thus reducing its relative contribution to Eq. (13).

(3) Introducing symmetric elements between parts of the network may lead to a complete balancing between the two contributions in the numerator of Eq. (13).

In Fig. 1 we illustrate three possible ways to realize these strategies to mitigate the impact of the failure of a single link (red) in a real power grid. All three strategies provide significant relief to the right module of the Scandinavian power grid, which represents Finland, after a link failure occurred in the left module. Remarkably, all these strategies are intimately related to the graph's topological properties as we will see in the following sections.

### A. The role of the rerouting distance

With Eq. (13) expressing LODFs using STs at hand it is intuitively clear that certain paths in the network should play an important role in predicting the overall effect of line outages. In particular, we can see immediately that for a given failing link  $e_k$ , the numerator in Eq. (13) depends on the paths going through the link monitoring the flow changes  $e_l$  whereas the denominator does not. Therefore we expect the flow changes to be smaller on another link  $e_m$  that has a longer minimum path going through  $e_m$  and  $e_k$  compared with link  $e_l$ . This is due to the fact that reducing the number of possible paths in the sum over all STs  $\mathcal{N}^*(r, a \to b, s)$  effectively reduces the number of STs by fixing a certain path.

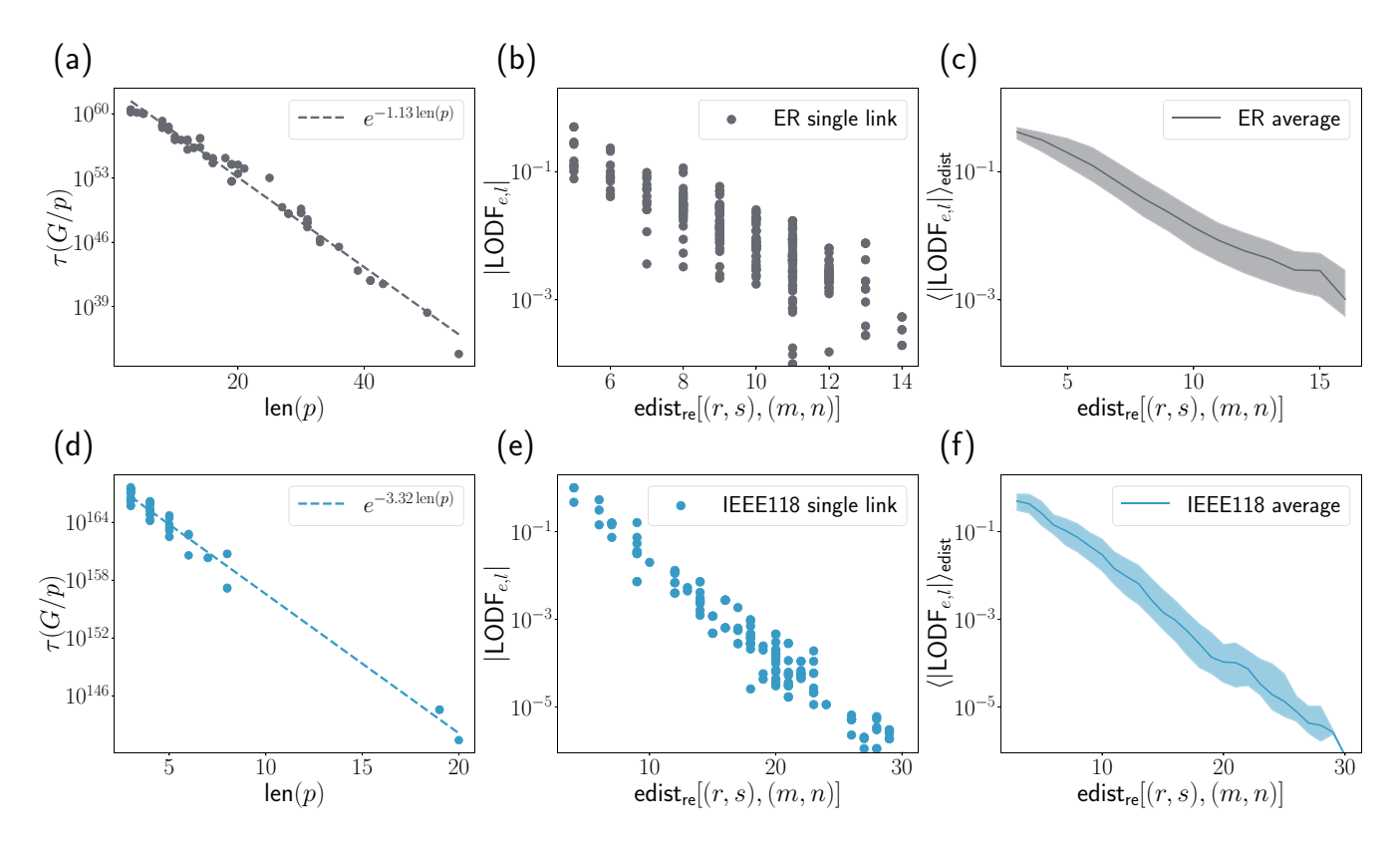


FIG. 2. Flow changes decay exponentially with cyclic paths in different networks. (a) and (d) Number of spanning trees (STs)  $\tau(G/p)$  in an Erdős-Rényi (ER) random graph G(200, 300) with 300 edges and 200 vertices (a) and in the power flow test case "IEEE 118" [35] (d) that contain a randomly chosen cyclic path p (y axis) plotted against the length of the path len(p) (x axis). The number of STs decays exponentially with the length of the path, thus appearing linear on a logarithmic y scale. (b) and (e) The rerouting distance scales exponentially with the LODF evaluated here for a single trigger for both grids. (c) and (f) The exponential scaling is preserved when averaging over all possible trigger links. Shading indicates 0.25 and 0.75 quantiles, a line represents the median. In Figs. 8 and 9 in the Appendix we demonstrate that the scaling robustly occurs for ER random graphs by analyzing 20 random realizations.

This intuitive idea is demonstrated to hold also quantitatively in Figs. 2(a) and 2(d): We illustrate that the number of STs  $\tau(G/p)$  scales approximately exponentially with the length of the cyclic path contained in the STs for an unweighted Erdős-Rényi (ER) random graph G(200, 300) with 300 edges and 200 vertices [36] [Fig. 2(a)] and the power flow test case "IEEE 118" [35,37] [Fig. 2(d)]. To study this scaling, we contract a cyclic path p between two arbitrarily chosen edges and quantify the number of STs using Kirchhoff's matrix tree theorem [8]. The theorem states that the number of STs in a graph may be calculated using the determinant of the graph's Laplacian matrix [7]

$$\tau(G)=\det(L_u).$$

Here,  $L_u$  is the matrix obtained from the Laplacian matrix L of G obtained by removing the row and column corresponding to an arbitrarily chosen vertex  $u \in V(G)$ . The number of STs  $\tau(G/p)$  containing a path p may be calculated by contracting the path in the graph and the Laplacian matrix and then taking the determinant of the resulting Laplacian. Taking the difference in the numerator of Eq. (13) between the path and a reversed path will in general not affect the exponential scaling since the difference of two exponential functions with different exponents or different prefactors will again scale exponentially. In Fig. 8 in the Appendix, we show

that the same scaling robustly occurs in ER random graphs by analyzing it for 20 different random realizations of ER graphs.

We may thus expect an exponential decay of LODFs with the length of fixed, cyclic paths. This result complements recent progress made in the understanding of the role played by distance for failure spreading in linear flow networks. In Ref. [12], it was shown that flow changes after a link failure are not captured well by the ordinary graph distance between the failing link and the link monitoring flow changes. Instead, a different distance measure referred to as rerouting distance captures this effect much better. It is defined as follows:

Definition 1. A rerouting path from vertex r to vertex s via the edge (m, n) is a path

$$(v_0 = r, v_1, \dots, v_i = m, v_{i+1} = n, v_{i+2}, \dots, v_k = s)$$

01

$$(v_0 = r, v_1, \dots, v_i = n, v_{i+1} = m, v_{i+2}, \dots, v_k = s)$$

where no vertex is visited twice. The *rerouting distance* between two edges (r, s) and (m, n) denoted by

$$edist_{re}[(r, s), (m, n)]$$

is the length of the shortest rerouting path from r to s via (m, n) plus the length of edge (r, s). Equivalently, it is the length of the shortest cycle crossing both edges (r, s) and

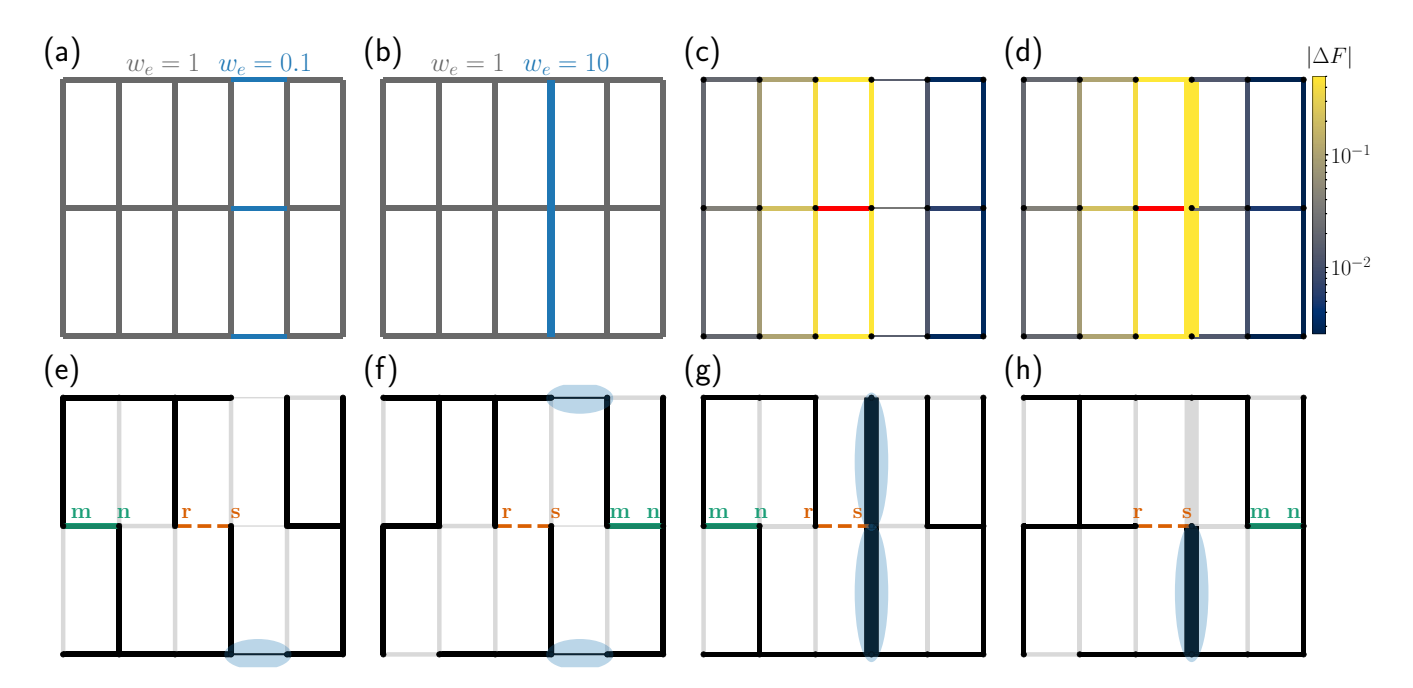


FIG. 3. Spanning trees (STs) may be used to explain the shielding effect of certain connectivity structures between different parts of a network. (a) and (b) A square grid is divided into two parts by either weakening the links connecting two parts [(a), blue,  $w_e = 0.1]$  or strengthening the links perpendicularly separating the two parts [(b), blue,  $w_e = 10]$ . (c) and (d) For both divisions, the failure of a single link with unit flow (red) significantly reduces failure spreading to the other part of the network. (e)–(h) Different STs (black) that contain specific paths of the form  $(v_0 = r, v_1, \ldots, v_i = m, v_{i+1} = n, v_{i+2}, \ldots, v_k = s)$  used to calculate the flow changes on link (m, n) for a failure of link (r, s) by virtue of Eq. (7). (e) and (f) For the weakly connected network shown in (a) and (c), a monitoring link in the same part (e) may lead to STs that contain only one weak link (blue shading). Thus the contribution of this ST to the sum over all STs is much stronger than for a monitoring link in the other part, where STs have to contain at least two weak links [(f), blue shading]. (g) and (h) For the strongly connected network shown in (g) and (h), the STs with the highest contribution are the ones containing all edges with strong weights [(g), blue shading]. (h) If links (m, n) and (r, s) are in different parts, no ST may contain all edges with strong weights (blue shading), thus reducing failure spreading in this case.

(m, n). If no such path exists, the rerouting distance is defined to be  $\infty$ .

Note that we include the weight of the edge (r, s) to make sure the rerouting distance is symmetric. The rerouting distance defined this way is a proper distance metric as shown in Ref. [12]. With the arguments made before at hand it is intuitively clear why the rerouting distance performs very well in predicting the effects of line outages. Indeed, we observe an exponential scaling of the LODFs for a given trigger link in the ER random graph [Fig. 2(b)] and in the test case "IEEE 118" [Fig. 2(e)]. The same observation still holds if we average over all monitoring links located at a fixed rerouting distance to the possible trigger links over which we average thereafter [Figs. 2(c) and 2(f)]. In Fig. 9 we show that the observed scaling robustly appears by comparing it for 20 different realizations of ER random graphs.

#### B. The role of strong and weak network connectivity

Our second strategy to reduce failure spreading after link failures is based on fixing specific paths in the network in such a way that they cannot contain certain links with large weights. This way, the numerator in Eq. (13) does not contain the contribution of the links with large weights whereas the denominator does, thereby reducing the overall impact of the link failure. Note that in contrast to the last section, the fixed

paths do not necessarily have to be long to prevent failure spreading. We will demonstrate this strategy for two cases: First, we use this reasoning to demonstrate that weakening the links between two parts of the network—thus effectively dividing it into communities—may reduce failure spreading between them. This is expected as weakly connected networks generally suppress failure spreading from one part to the other one, but this also limits the possibility of power flow between the parts. This is no longer true for the second strategy: We illustrate why also strengthening the links that separate two parts of the network perpendicularly to the community boundary reduces the impact of link failures.

The two strategies are illustrated for a simple  $3 \times 6$  square grid in Fig. 3. We divide the square grid into two parts by either weakening the links that separate the parts [Fig. 3(a)] or strengthening the links perpendicular to these links [Fig. 3(b)]. We then monitor the flow changes (color scale) after the failure of a single link (red) in both cases [Figs. 3(c) and 3(d)]. For weak connectivity, the failure of link  $e_k = (r, s)$  (dashed orange line) leads to a different contribution of the numerator in Eq. (13) if the monitoring link  $e_\ell = (m, n)$  (green line) is contained in the same part [Fig. 3(e)] as compared with a different, weakly connected part [Fig. 3(f)] in an otherwise symmetrical situation. Note that the distance between monitoring link and trigger link is also the same in both Fig. 3(e) and Fig. 3(f). For a link in the same part, the numerator also

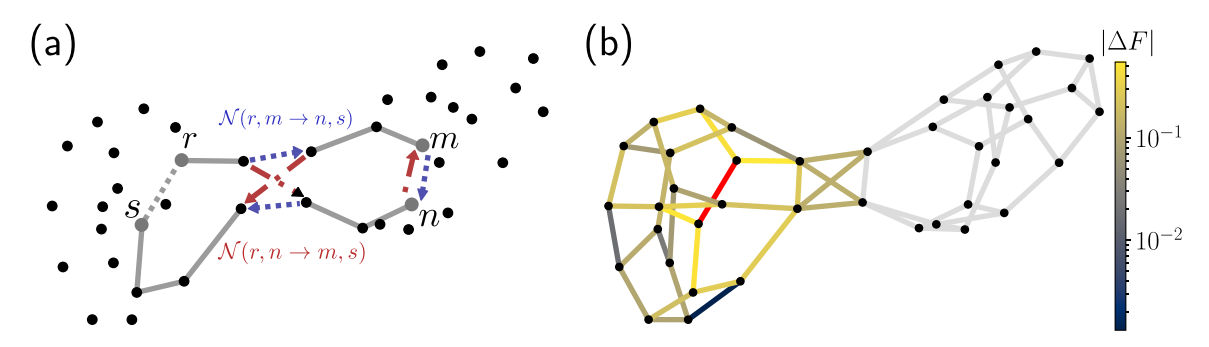


FIG. 4. Network isolators that lead to a complete vanishing of LODFs are created using certain symmetric paths in the network. (a) STs that contain a path starting at node r and terminating at node s and containing the edge (m, n) (blue) or (n, m) (red) have to cross the subgraph consisting of dotted, colored edges in the center. Since each path can contain each vertex and edge only once, each ST passing through the subgraph in one way (blue) has a counterpart passing through the subgraph in the other way (red). (b) Failure of a link (red) results in vanishing LODFs (color scale) in the part connected by a network isolator as predicted using the ST formulation of link failures.

contributes with STs containing only *one* weak link (thin line, blue shading). For a trigger link located in the other part, each ST connecting trigger link and monitoring link has to contain at least *two* weak links (shaded blue). Since the contribution in the numerator is proportional to the product of all weights along the ST and the situation is otherwise symmetric, we expect a weaker LODF and thus a shielding effect if the two links are contained in different, weakly connected parts.

A similar observation holds in the case of strong connectivity: If the monitoring link  $e_{\ell} = (m, n)$  is contained in the same part of the network as the trigger link  $e_k = (r, s)$  [Fig. 3(g)], now separated through strong connections, spanning trees connecting the two links may contain two—or generally, all—strong links. For a trigger link in the other part of the network, the spanning tree connecting them can contain maximally one—or generally, all minus one—strong links. Again, the term in the numerator scales with the link weights contained in the spanning trees. Therefore we expect the effect of link failures to be stronger for links located in the same part as compared with links contained in the other part, which is confirmed when simulating the failure of a single link in Fig. 3(d).

## C. The role of symmetry

As a third strategy for reducing failure spreading, we suggest building networks in such a way that the terms in the numerator of Eq. (13) balance. In this case, failure spreading reduces to zero for the respective links. In order to balance the terms in the numerator of Eq. (13), we need the spanning trees passing through the monitoring link  $e_{\ell} = (a, b)$  in both directions to have exactly the same weight

$$\mathcal{N}^*(r, m \to n, s) = \mathcal{N}^*(r, n \to m, s)$$

$$\Rightarrow \sum_{T \in \mathcal{T}(r, m \to n, s)} \prod_{e \in T} w_e = \sum_{T \in \mathcal{T}(r, n \to m, s)} \prod_{e \in T} w_e.$$

Here,  $\mathcal{T}(r, m \to n, s)$  is the set of all spanning trees containing a path of the form  $(r, \ldots, m, n, \ldots, s)$ . This equality is, for example, fulfilled if for each tree  $T \in \mathcal{T}(r, m \to n, s)$  there is a counterpart  $T \in \mathcal{T}(r, n \to m, s)$  of the same weight. This may be accomplished by introducing certain symmetric elements, referred to as *network isolators* [19], into the

graph as demonstrated in Fig. 4: For each ST connecting trigger link  $e_k = (r, s)$  and monitoring link  $e_\ell = (m, n)$  and containing a path of the form  $(r, \ldots, m, n, \ldots, s)$  (gray and blue lines) there is an ST containing a path of the form  $(r, \ldots, n, m, \ldots, s)$  (gray and red lines). If we compare the product of weights for a single tree  $T_0 \in \mathcal{T}(r, m \to n, s)$  and its counterpart  $T_0^* \in \mathcal{T}(r, n \to m, s)$ , such that both contain exactly the same edges except for the edges connecting the two parts, i.e., the links marked as blue and red arrows in Fig. 4(a), we can see that these products are equal except for the links  $r_1$  and  $r_2$  (red links) being contained only in  $T_0$ , and  $b_1$  and  $b_2$  (blue links) being contained only in  $T_0^*$ . We can thus conclude that the above equality is fulfilled, i.e., the product of weights is equal for both trees  $T_0$  and  $T_0^*$ , if

$$b_1 \cdot b_2 = r_1 \cdot r_2$$
.

In this case, a failure of link  $e_k = (r, s)$  does not result in any flow changes on link  $e_\ell = (m, n)$  at all. This reasoning has been generalized recently, where the concept was termed *network isolators* [19]. We also note that similar arguments were put forward by Guo *et al.* [16]. On general grounds, network isolators are defined as follows [19].

Lemma 2. Consider a linear flow network consisting of two parts with vertex sets  $V_1$  and  $V_2$  and assume that a single link in

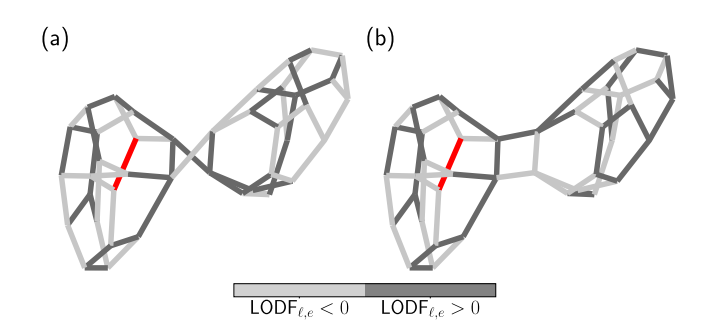


FIG. 5. Sign reversal of LODFs by symmetric subgraphs. (a) and (b) Modifying the subgraph connecting two graphs from the two parallel lines to the two crossing lines leads to a sign reversal of the LODFs in the connecting subgraphs (shades of gray). This is in line with the compensatory effect of the symmetric subgraphs used to create the network isolator in Fig. 4.

the induced subgraph  $G(V_1)$  fails, i.e., a link (r, s) with  $r, s \in V_1$ . If the adjacency matrix of the mutual connections has unit rank  $(\mathbf{A}_{12}) = 1$ , then the flows on all links in the induced subgraph  $G(V_2)$  are not affected by the failure; that is,

$$\Delta F_{m,n} \equiv 0 \quad \forall m, n \in V_2.$$

The subgraph corresponding to the mutual interactions is referred to as a *network isolator*.

Note that network isolators of arbitrary size may be understood using the same reasoning as presented above for a network isolator consisting of only four links.

### 1. Sign reversal of flow changes

Based on the symmetric elements—the network isolators—introduced in Sec. IV C, we can demonstrate yet another application of the ST formulation to link failures: We can modify the grid in such a way that the LODFs and thus the flow changes change their sign. This is again based on the symmetry of LODFs in terms of the paths  $(r, \ldots, m, n, \ldots, s)$  and  $(r, \ldots, n, m, \ldots, s)$ . If we apply a symmetric modification such that paths of the first form are replaced by parts of the latter one, we can reverse the sign of the resulting flow changes in the other part. In particular, if we interchange the two terms appearing in the nominator of Eq. (13) for a subset of edges, we can change the sign of the LODF for these edges

$$\mathcal{N}^*(r, m \to n, s) \to \mathcal{N}^*(r, n \to m, s)$$
$$\mathcal{N}^*(r, n \to m, s) \to \mathcal{N}^*(r, m \to n, s)$$
$$\Rightarrow LODF_{\ell,k} \to -LODF_{\ell,k}.$$

This can be achieved using a modification similar to the one shown in Fig. 4(a): If the initial network contains the subgraph indicated by blue dashed arrows in the center, we can revert the sign of the LODF $_{\ell,k}$  by changing this subgraph to the one indicated by red dashed arrows. This is demonstrated in Fig. 5: Changing the subgraph in the center connecting the two graphs from the "x"-shaped subgraph [Fig. 5(a)] to the "="-shaped subgraph [Fig. 5(b)] leads to a sign reversal of the LODFs in the second graph (shades of gray), while the magnitude of LODFs is the same in both panels. This modification thus allows us to simultaneously change the sign of all LODFs in a subgraph, which may prevent overloads that are caused by flows going in a particular direction.

# D. Comparison of strategies for mitigating failure spreading

Our theoretical analysis has led to three different strategies to mitigate failure spreading by optimizing the network topology. We will now quantify to what extent these modifications in topology improve the overall network resilience in terms of the impact of a single line failure.

To begin with, we quantify the suppression of failure spreading between two preselected parts of the network. As an indicator we use the ratio of the LODFs evaluated at a given distance d to the failing link m suggested in Ref. [19]

$$R(m,d) = \frac{\langle |\text{LODF}_{k,m}| \rangle_d^{e_k \in O}}{\langle |\text{LODF}_{k,m}| \rangle_d^{e_k \in S}}.$$
 (14)

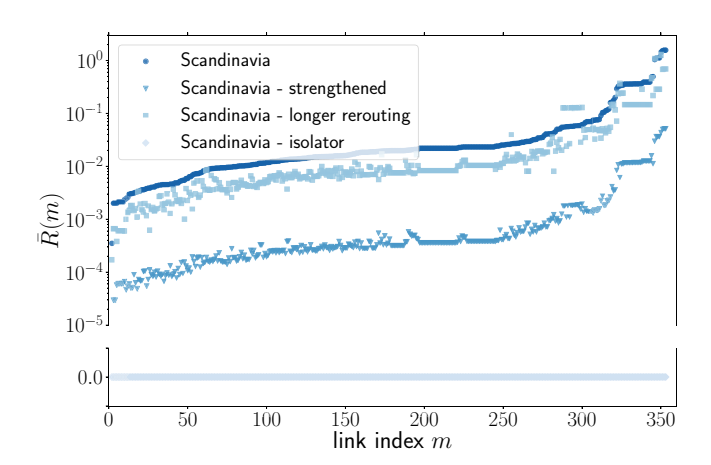


FIG. 6. Failure spreading between Finland and the rest of Scandinavia is suppressed for all three strategies. We evaluate the ratio of LODFs,  $\bar{R}(m) := \langle R(m,d) \rangle_d$ , averaged over distance d [Eq. (14)] between the right part of the grid, i.e., Finland, and its left part, i.e., the remainder of Scandinavia (see Fig. 1). We average the ratio over all distances d for a given trigger link m and sort the values by magnitude for the initial Scandinavian power grid (dark blue circles). We then analyze the ratio for the three strategies outlined in Sec. IV B and shown in Fig. 1. We observe that all strategies consistently yield reduced failure spreading between the two parts. Strengthening a specific link [blue triangles; cf. Fig. 1(b)] inhibits failure spreading more than increasing the length of the rerouting path [light blue squares; cf. Fig. 1(c)], while adding a network isolator [light blue diamonds; cf. Fig. 1(d)] completely suppresses failure spreading.

Here, O and S are the two preselected parts of the network that are supposed to be protected against each other in terms of failure spreading,  $m \in S$  is the failing link located in part S, and d is the unweighted edge distance between trigger link m and monitoring link k. We average the absolute LODF over all links k located in the other (O, numerator) and the same (S, denominator) part located at the fixed distance d. The ratio assumes values between  $R \approx 1$  if LODFs in both parts assume similar values and  $R \approx 0$  if failure spreading to the other part O is suppressed completely.

In Fig. 6 we analyze to what extent the three strategies shown in Fig. 1 are able to reduce failure spreading between Finland and the remainder of Scandinavia. We analyze the LODF ratio for all possible trigger links m that are present in both the modified and the initial grid and compare the ratio for a given link by averaging the ratio over the distance d. Thereby, we are able to compare to what extent failure spreading caused by the failure of a given link is reduced in each grid modification scenario. We observe that all three strategies consistently suppress failure spreading to the other part as measured by a reduction in the LODF ratio. Whereas strengthening a single link [Fig. 1(b)] suppresses spreading more strongly than an increase in rerouting [Fig. 1(c)], adding a network isolator [Fig. 1(d)] provides the strongest reduction in failure spreading by setting the LODF ratio to zero.

While all three strategies suppress failure spreading *between* the two parts, we did not yet consider their overall impact on the entire network, i.e., including their impact on the same part where the trigger link is located. To quantify the

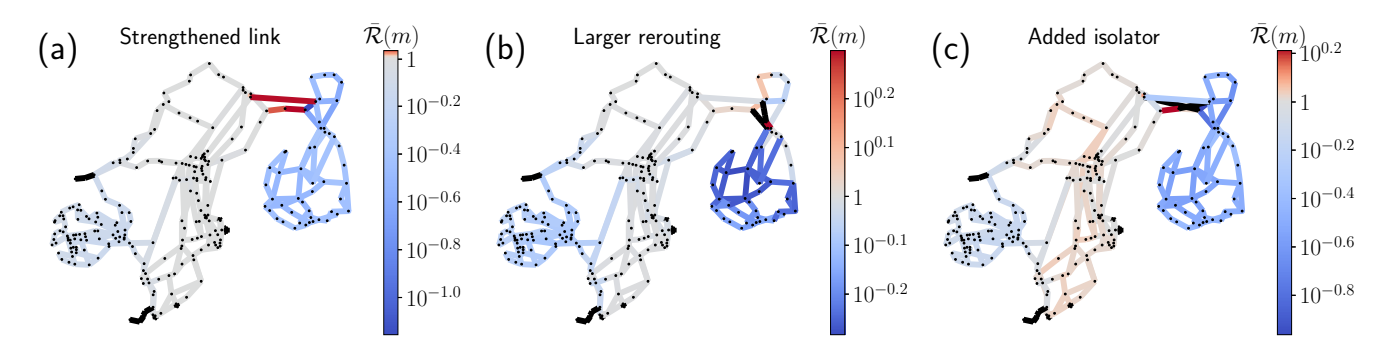


FIG. 7. Systematic analysis of the overall impact of a given strategy for mitigating failure spreading. We compare the impact of each of the strategies shown in Fig. 1 on the overall grid resilience measured by the LODF ratio  $\bar{\mathcal{R}}(m) := \langle \mathcal{R}(m,d) \rangle_d$  averaged over distance d [Eq. (15)], which expresses to what extent the impact of the failure of a given link m on the network differs from its impact in the grid without the modification. We average the ratio over all distances to calculate a link-based measure of grid resilience. (a) We observe that strengthening a single link has an overall positive impact on grid resilience and reduces the LODF ratio up to tenfold (dark blue links), with only a few links showing an increase (red). (b) An increase in rerouting as shown in Fig. 1(c) improves resilience in most links as well; the effect is, however, less pronounced than in the previous case. (c) Adding a network isolator strongly improves resilience in Finland, while slightly weakening it in the rest of Scandinavia. Thus all three strategies consistently have a positive impact on link-based resilience in Finland.

overall impact, we now consider the ratio of LODFs before and after the grid modification

$$\mathcal{R}(m,d) = \frac{\langle |\text{LODF}_{k,m}| \rangle_d^{e_k \in G'}}{\langle |\text{LODF}_{k,m}| \rangle_d^{e_k \in G}}.$$
 (15)

Here, G is the initial network, and G' is the network after the topology has been modified according to a chosen strategy. As before, m denotes the failing link, and the magnitudes of the LODFs are averaged over all links k at a given distance d to the trigger link m. Only links which are present in both G and G' are considered as trigger links. While being defined similarly to the ratio of LODFs in Eq. (14), the main difference between the two quantities is the following: The ratio considered here compares the impact of a link failure in two different networks, while the ratio in Eq. (14) compares the impact on two different parts of the same network. The ratio defined here thus quantifies whether a given modification leads to lower average LODFs in the entire grid or whether it increases the vulnerability of some links. It assumes values of unity,  $\mathcal{R}(m,d) \approx 1$ , if the impact of the failure on the entire grid is approximately the same in the initial and the modified grid and deviates from unity if the impact of a failure of the given link m on links at a distance d is reduced  $[\mathcal{R}(m, d) < 1]$ or increased  $[\mathcal{R}(m, d) > 1]$ .

In Fig. 7, we analyze this ratio for the Scandinavian grid for each strategy and the resulting grid modification at the border between Finland and the remainder of Scandinavia shown in Fig. 1. To be precise, we evaluate the distance-averaged LODF ratio  $\bar{\mathcal{R}}(m) := \langle \mathcal{R}(m,d) \rangle_d$  for all possible trigger links m. For all three strategies, we observe a reduction in failure spreading, i.e.,  $\bar{\mathcal{R}}(m) < 1$ , if the trigger link m is located in the bulk of Finland or in western Norway. The benefits are strongest if a network isolator is added [Fig. 7(c)] and weakest if rerouting distance is increased [Fig. 7(b)]. For a trigger link m located in the central part of the grid, i.e., in Sweden, the addition of an isolator has a slightly negative effect such that  $\bar{\mathcal{R}}(m) > 1$ , which is, however, much weaker than the positive effects on the other parts of the grid. The

two other strategies have a negligible impact if *m* is in this part of the grid. In all cases, the ratio indicates an increase in failure spreading for a few trigger links that are located in the vicinity of the topology modification. To conclude, we observe that the choice of a favorable strategy depends on the goal to be achieved. If trigger links in Sweden or in the vicinity of the border between Sweden and Finland have been identified as links that are likely to fail, none of the strategies will strongly increase grid resilience or will even deplete it. If, on the other hand, the goal is to protect the grid against likely link failures that emerge in Finland, all three strategies consistently provide a certain benefit to grid resilience which is also confirmed by the results in Fig. 6. In this case, adding a network isolator most likely provides the best results.

In total, the LODF ratios R(m, d) and  $\mathcal{R}(m, d)$  provide a complementary view on the different strategies by measuring the extent to which failures are suppressed between the two parts of a network, on the one hand, and the impact of a strategy on the network as a whole on the other one. For this reason, they can be used to balance the pros and cons of a grid modification and thus allow one to find which strategy performs best for the given grid or even allow one to study the impact of a combination of different strategies.

### V. CONCLUSION

We demonstrated how a spanning tree formulation of link failures may be used to understand which topological patterns aid the mitigation of failure spreading in power grids and other types of linear flow networks. In particular, we derived and explained three strategies for reducing the effect of link failures in linear flow networks based on spanning trees. Our results offer an understanding of previous strategies used to inhibit failure spreading in power grids and may thus help to increase power grid security.

All strategies analyzed here for reducing failure spreading are based on extending—or at least not reducing—the network's ability to transport flows. This is in contrast to typical containment strategies in power grid security which are based

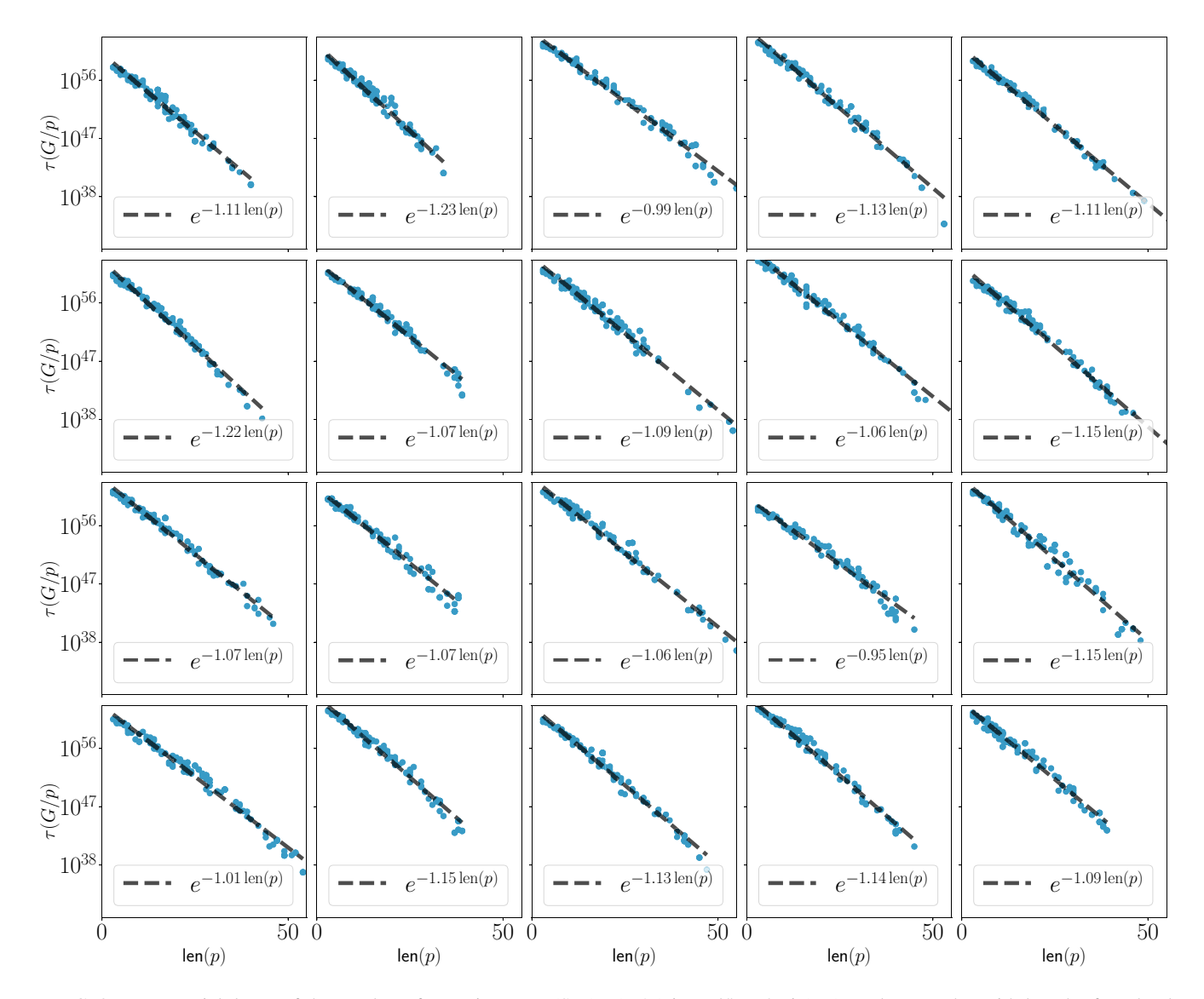


FIG. 8. Exponential decay of the number of spanning trees (STs)  $\tau(G/p)$  in Erdős-Rényi (ER) random graphs, with length of randomly chosen cyclic path len(p), occurs robustly. Each panel shows the number of STs in a different, random realization of an ER graph G(200, 300) with 300 edges and 200 vertices after collapsing a randomly chosen cyclic path. We analyze 200 randomly chosen cyclic paths for each ER graph (dots) and perform a least-squares fit of an exponential function on the semilog scale (dashed lines). The number of STs decays exponentially with the length of the path, thus appearing linear on a logarithmic y scale.

on islanding the power grid, i.e., reducing the connectivity for the sake of security. We illustrated how to exploit the intimate connection to graph theory to find and analyze subgraphs that allow for improving both power grid resilience and efficiency at the same time.

Our results offer a new understanding on a graphtheoretical level of network structures that have been found to inhibit or enhance failure spreading. We illustrated the fruitful approach of analyzing failure spreading in power grids by using spanning trees for several subgraphs but are confident that other subgraphs for enhancing or inhibiting failure spreading may be unveiled using this formalism.

Finally, the question arises regarding to what extent our theoretical results are relevant for the stability of real-world power grids, in particular, the stability to large-scale blackouts. In fact, a power grid blackout is typically triggered by the outage of a single transmission element, more rarely a single generation element [21]. When such a transmission line outage occurs, power flow is redistributed to parallel transmission paths, which may cause secondary overloads. Hence the scenario considered in this paper is of high practical relevance.

Our results have been derived for the linearized dc approximation; hence they will hold only approximately for scenarios where the dc approximation is no longer valid. In particular, there is no longer an exact analogy between resistor networks and ac power grids when flows are calculated nonlinearly using ac power flow models. However, the impact of line failures in high-voltage grids is typically well described by the linearized dc approximation [19,34]. Deviations occur mainly for high-loading scenarios, but even then the dc approximation usually gives a reasonable first-order estimate of the flow redistribution. It must be noted that the assumptions leading

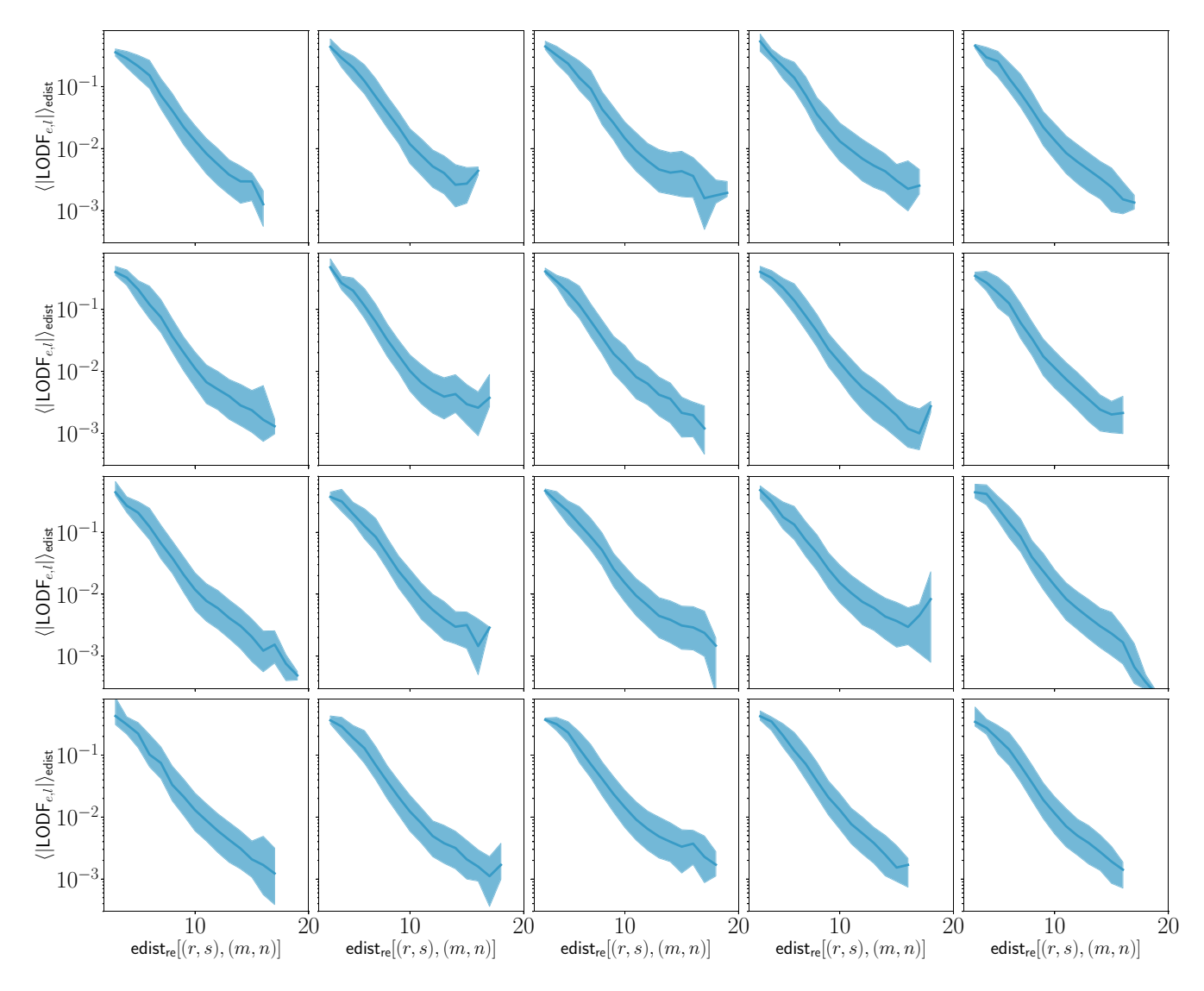


FIG. 9. Decay of averaged LODFs with rerouting distance to the trigger link is robust throughout 20 different realizations of Erdős-Rényi (ER) random graphs. Each panel shows the decay of LODFs for a different, random realization of an ER graph G(200, 300) with 300 edges and 200 vertices. We observe an approximately exponential scaling of LODFs with rerouting distance when averaging over all possible links located at a fixed rerouting distance to the trigger link. Shading indicates 0.25 and 0.75 quantiles; a line represents the median.

to the dc approximation are not necessarily violated during the initial stages of a cascade. Secondary overloads occur when the current or real power flow exceeds a threshold. If the reactance  $x_\ell$  is not too large, this will happen well before the angle difference becomes large. During the final stages of a cascade, nonlinear and dynamical effects must be taken into account

Nevertheless, the focus of our study is on flow networks where flow distribution and redistribution after failures are governed by Kirchhoff's laws. Further studies are necessary to assess whether parts of our results may in some sense be transferred to topological models where flows are routed along shortest paths [38–40].

## ACKNOWLEDGMENTS

We gratefully acknowledge support from the German Federal Ministry of Education and Research (Grant No. 03EK3055B) and the Helmholtz Association (via the joint initiative "Energy System 2050 – A Contribution of the Research Field Energy" and Grant No. VH-NG-1025).

### **APPENDIX**

In this Appendix, we demonstrate that the scaling robustly occurs for ER random graphs by analyzing 20 random realizations (Figs. 8 and 9).

- [1] N. Hwang and R. Houghtalen, Fundamentals of Hydraulic Engineering Systems (Prentice-Hall, Upper Saddle River, NJ, 1996).
- [2] S. Díaz, J. González, and R. Mínguez, Observability analysis in water transport networks: Algebraic approach, J. Water Resour. Plann. Manage. 142, 04015071 (2016).
- [3] F. Corson, Fluctuations and Redundancy in Optimal Transport Networks, Phys. Rev. Lett. 104, 048703 (2010).
- [4] E. Katifori, G. J. Szöllősi, and M. O. Magnasco, Damage and Fluctuations Induce Loops in Optimal Transport Networks, Phys. Rev. Lett. 104, 048704 (2010).
- [5] D. Hu and D. Cai, Adaptation and Optimization of Biological Transport Networks, Phys. Rev. Lett. 111, 138701 (2013).
- [6] F. Kaiser, H. Ronellenfitsch, and D. Witthaut, Discontinuous transition to loop formation in optimal supply networks, Nat. Commun. 11, 5796 (2020).
- [7] B. Bollobás, Modern Graph Theory, Graduate Texts in Mathematics Vol. 184 (Springer, New York, 1998).
- [8] G. Kirchhoff, Ueber die Auflösung der Gleichungen, auf welche man bei der Untersuchung der linearen Vertheilung galvanischer Ströme geführt wird, Ann. Phys. (Berlin) 148, 497 (1847).
- [9] P. Van Mieghem, K. Devriendt, and H. Cetinay, Pseudoinverse of the Laplacian and best spreader node in a network, Phys. Rev. E 96, 032311 (2017).
- [10] D. Van Hertem, J. Verboomen, K. Purchala, R. Belmans, and W. Kling, Usefulness of DC power flow for active power flow analysis with flow controlling devices, in *The 8th IEE International Conference on AC and DC Power Transmission* (IEE, London, 2006), pp. 58–62.
- [11] A. J. Wood, B. F. Wollenberg, and G. B. Sheblé, *Power Generation, Operation and Control* (John Wiley, New York, 2014).
- [12] J. Strake, F. Kaiser, F. Basiri, H. Ronellenfitsch, and D. Witthaut, Non-local impact of link failures in linear flow networks, New J. Phys. 21, 053009 (2019).
- [13] F. Kaiser, J. Strake, and D. Witthaut, Collective effects of link failures in linear flow networks, New J. Phys. 22, 013053 (2020).
- [14] T. Gavrilchenko and E. Katifori, Resilience in hierarchical fluid flow networks, Phys. Rev. E **99**, 012321 (2019).
- [15] H. Cetinay, F. A. Kuipers, and P. V. Mieghem, A topological investigation of power flow, IEEE Syst. J. 12, 2524 (2018).
- [16] L. Guo, C. Liang, and S. H. Low, Monotonicity properties and spectral characterization of power redistribution in cascading failures, in 2017 55th Annual Allerton Conference on Communication, Control, and Computing (Allerton) (IEEE, Piscataway, NJ, 2017), pp. 918–925.
- [17] L. Guo, C. Liang, A. Zocca, S. H. Low, and A. Wierman, Line failure localization of power networks Part II: Cut set outages in *IEEE Transactions on Power Systems* (IEEE, 2021).
- [18] L. Guo, C. Liang, A. Zocca, S. H. Low, and A. Wierman, Line failure localization of power networks Part I: Non-cut outages, in *IEEE Transactions on Power Systems* (IEEE, 2021).
- [19] F. Kaiser, V. Latora, and D. Witthaut, Network isolators inhibit failure spreading in complex networks, Nature Commun. 12, 3143 (2021).
- [20] J. C. Maxwell, *A Treatise on Electricity and Magnetism*, Cambridge Library Collection - Physical Sciences Vol. 2 (Cambridge University Press, Cambridge, 2010).

- [21] P. Pourbeik, P. Kundur, and C. Taylor, The anatomy of a power grid blackout Root causes and dynamics of recent major blackouts, IEEE Power Energy Mag. 4, 22 (2006).
- [22] D. Witthaut and M. Timme, Nonlocal effects and countermeasures in cascading failures, Phys. Rev. E 92, 032809 (2015).
- [23] Y. Yang, T. Nishikawa, and A. E. Motter, Small vulnerable sets determine large network cascades in power grids, Science 358, eaan3184 (2017).
- [24] V. Belevitch, Summary of the history of circuit theory, Proc. IRE **50**, 848 (1962).
- [25] N. Biggs, Algebraic potential theory on graphs, Bull. London Math. Soc. 29, 641 (1997).
- [26] R. Diestel, *Graph Theory* (Springer, New York, 2010).
- [27] E. H. Moore, On the reciprocal of the general algebraic matrix, Bull. Am. Math. Soc. 26, 394 (1920).
- [28] L. W. Shapiro, An electrical lemma, Math. Mag. 60, 36 (1987).
- [29] K. Purchala, L. Meeus, D. V. Dommelen, and R. Belmans, Usefulness of DC power flow for active power flow analysis, in *IEEE Power Engineering Society General Meeting* (IEEE, Piscataway, NJ, 2005), Vol. 1, pp. 454–459.
- [30] J. Hörsch, F. Hofmann, D. Schlachtberger, and T. Brown, PyPSA-Eur: An open optimisation model of the European transmission system, Energy Strategy Rev. 22, 207 (2018).
- [31] D. Manik, M. Rohden, H. Ronellenfitsch, X. Zhang, S. Hallerberg, D. Witthaut, and M. Timme, Network susceptibilities: Theory and applications, Phys. Rev. E 95, 012319 (2017).
- [32] M. Korkali, J. G. Veneman, B. F. Tivnan, J. P. Bagrow, and P. D. H. Hines, Reducing cascading failure risk by increasing infrastructure network interdependence, Sci. Rep. 7, 44499 (2017).
- [33] T. Nesti, F. Sloothaak, and B. Zwart, Emergence of Scale-Free Blackout Sizes in Power Grids, Phys. Rev. Lett. 125, 058301 (2020).
- [34] H. Cetinay, S. Soltan, F. A. Kuipers, G. Zussman, and P. V. Mieghem, Comparing the effects of failures in power grids under the AC and DC power flow models, IEEE Trans. Network Sci. Eng. 5, 301 (2018).
- [35] R. D. Zimmerman, C. E. Murillo-Sanchez, and R. J. Thomas, MATPOWER: Steady-state operations, planning and analysis tools for power systems research and education, IEEE Trans. Power Syst. 26, 12 (2011).
- [36] P. Erdős and A. Rényi, On the evolution of random graphs, Publ. Math. Inst. Hung. Acad. Sci. 5, 17 (1960).
- [37] C. Josz, S. Fliscounakis, J. Maeght, and P. Panciatici, AC power flow data in MATPOWER and QCQP format: iTesla, RTE snapshots, and PEGASE, arXiv:1603.01533 [math].
- [38] O. Artime and M. D. Domenico, Abrupt transition due to non-local cascade propagation in multiplex systems, New J. Phys. **22**, 093035 (2020).
- [39] A. E. Motter and Y.-C. Lai, Cascade-based attacks on complex networks, Phys. Rev. E 66, 065102(R) (2002).
- [40] P. Crucitti, V. Latora, and M. Marchiori, Model for cascading failures in complex networks, Phys. Rev. E **69**, 045104(R) (2004).